

Stress Control in ZnO Nanoparticle-based Discs via High-oxygen Thermal Annealing at Various Temperatures

Rabab Khalid Sendi* and Shahrom Mahmud

School of Physics, Universiti Sains Malaysia, 11800 USM
Pulau Pinang, Malaysia

*Corresponding author: Last-name3@hotmail.com

Abstract: *The stress and lattice constants in zinc oxide (ZnO) nanoparticles play a major role in determining the distortions that occur in the crystal during the preparation of the sample as a result of exposure to several factors, such as external strain, temperature, pressing and structural defects (oxygen vacancies and zinc/oxygen interstitials). ZnO nanoparticles (20 nm) were used to make high-density ZnO discs via uniaxial pressing at 4 ton cm^{-2} and sintering at 1200°C for 1 h. Structural, elemental and optical characterisations were then performed on the samples using various techniques. High-oxygen thermal annealing significantly affected the ZnO discs, particularly in enhancing the growth of the grain even at a low annealing temperature (450°C). The strong solid-state reaction during annealing may be attributed to the high surface area of the 20 nm ZnO nanoparticles that exhibited a strong surface reaction even at low annealing temperatures. The annealing treatment also improved the grain crystallinity, as shown by the transition of the intrinsic compressive stress to tensile stress based on the XRD lattice constant and full-width at half-maximum data. Therefore, high-oxygen thermal annealing can be used as a new technique in controlling the stress in nanoparticle-based ZnO discs and produce discs with improved structural and optical properties.*

Keywords: Annealing process, ZnO, nanoparticles, crystal growth, Raman spectroscopy, particle size

1. INTRODUCTION

Considerable interest has been focused on zinc oxide (ZnO) in recent years because of its wide direct bandgap and strong excitonic binding energy, which makes it a promising material for ultraviolet (UV) lasers with low thresholds,¹ field emission arrays,^{2,3} surfacial acoustic devices,⁴ and transistors and biosensors.⁵ Aside from the typical nanowire, nanorod, nanobelt and nanotube morphologies, other fascinating ZnO nanoparticle structures include the hierarchical and tetrapod nanowhiskers, nanocombs and nanopins, which have been synthesised via different routes.^{6,7}

Thermal annealing treatment is a widely used, effective technique for improving the crystalline quality of ZnO. The annealing temperature plays an

important role in controlling the intrinsic defects in ZnO and the properties of the samples. Recrystallisation can occur at higher annealing temperatures, and the concentration of the defects changes with the annealing temperature and the ambient atmosphere. Other important annealing parameters include the ambient gas, time and gas flow rate.

Previous studies⁸⁻¹¹ have shown that an optimum annealing treatment improves the crystal quality of ZnO and changes the Zn/O ratio as well as the intrinsic defects of the sample. Meanwhile, a number of studies have focused on determining the effect of thermal or oxygen partial pressures on the stress and structure of ZnO.^{12,13} These two parameters are known to strongly affect the residual stresses in ZnO discs. However, thermal annealing significantly affects the ZnO structure because thermal energy improves the crystallisation of ZnO discs.¹⁴ The stress arises during the growth process; hence, a perfect, stress-free crystallisation of ZnO can be achieved by adjusting the temperature and oxygen flow rates under optimal conditions. In other words, the intrinsic growth stress in the ZnO disc can be controlled by adjusting the conditions of the annealing process. The current study aims to demonstrate the conversion of stress from compressive to tensile during the annealing of ZnO discs by controlling the thermal annealing temperature at a fixed oxygen flow rate (2 L m^{-2}). The correlation between the stress during annealing and the lattice constant is also investigated. Therefore, this study presents the effect of high-oxygen thermal annealing at various temperatures on the stress and lattice constant of ZnO nanoparticle-based ZnO discs.

2. EXPERIMENTAL

ZnO discs were prepared via the conventional ceramic processing method involving ball milling, drying, pressing and sintering (1200°C). ZnO (20 nm) powder (MK Nano, > 99.8% purity) was obtained from the industry and used in producing ZnO discs.

ZnO nanopowder was blended with polyvinyl alcohol (PVA) by mixing with distilled water in a ball milling jar for 6 h. ZnO slurry was air-dried at 60°C for 1 h. The dried material was granulated by sieving through a 20-mesh sieve. The resulting granules were pressed under 4 ton cm^{-2} pressure to produce 26 mm wide and 3 mm thick green ZnO discs. Finally, the green discs were sintered at 1200°C in air for 1 h.

The as-grown ZnO samples were annealed in oxygen atmosphere at various temperatures from 450°C to 850°C for 1 h. The oxygen flow rate was 2 L min^{-1} .

The microstructure of the ZnO discs was examined using scanning electron microscopy (SEM) and Energy dispersive X-ray spectroscopy (EDX) system (model: JSM – 6460 LV) and the grain size was determined by the ZnO-ZnO grain boundary crossing method. The crystalline phases were studied using a high resolution X-ray diffractometer (XRD) equipment (PANalytical X' Pert PRO MED PW3040) with Cu K_{α} radiation ($\lambda = 1.5406 \text{ \AA}$). Room temperature photoluminescence (PL) spectra were obtained using a Jobin Yvon HR 800 UV spectrometer system at room temperature. Raman spectroscopy was conducted as a supplementary tool to identify structural information (514.5 nm, argon ion laser, Labram-HR).

3. RESULTS AND DISCUSSION

Figure 1 shows the SEM micrographs of unannealed and annealed ZnO discs at 450°C, 550°C, 650°C, 750°C and 850°C. The surface morphology of the samples strongly depended on the annealing temperature, indicating that the average grain size of ZnO increased with temperature. The as-grown ZnO discs consisted of co-joined grains (average grain size = 1.3 μm) and exhibited a highly porous morphology [Figure 1(a)].

The ZnO grains increased in size to approximately 1.4, 1.6, 1.9, 2.4 and 2.7 μm as the annealing temperature was increased to 450°C, 550°C, 650°C, 750°C and 850°C, respectively [Figures 1(b) to 1(f)]. The grains became more structurally arranged as they increased in size, resembling polygons/hexagons; at the same time, the porosity decreased, indicating that a higher annealing temperature promotes internal atomic diffusion, which is responsible for grain growth and pore elimination.

The ZnO nanoparticles had small-grains sized structures with the morphology changing according to the variation in the annealing temperatures. The SEM images show that the grain boundaries were fewer and the grains grew much bigger with further increase of annealing temperature. The high annealing temperature provides more activation energy to atoms to grow larger grains. Lin et al.³² described that high temperature can stimulate the migration of grain boundaries and cause the coalescence of more grains during the annealing processes. Fang et al.⁸ further indicated that at high temperature, more energy should be available for the atoms to acquire so that they may diffuse and occupy the correct site in the crystal lattice and grains with lower surface energy will grow larger at high temperature.

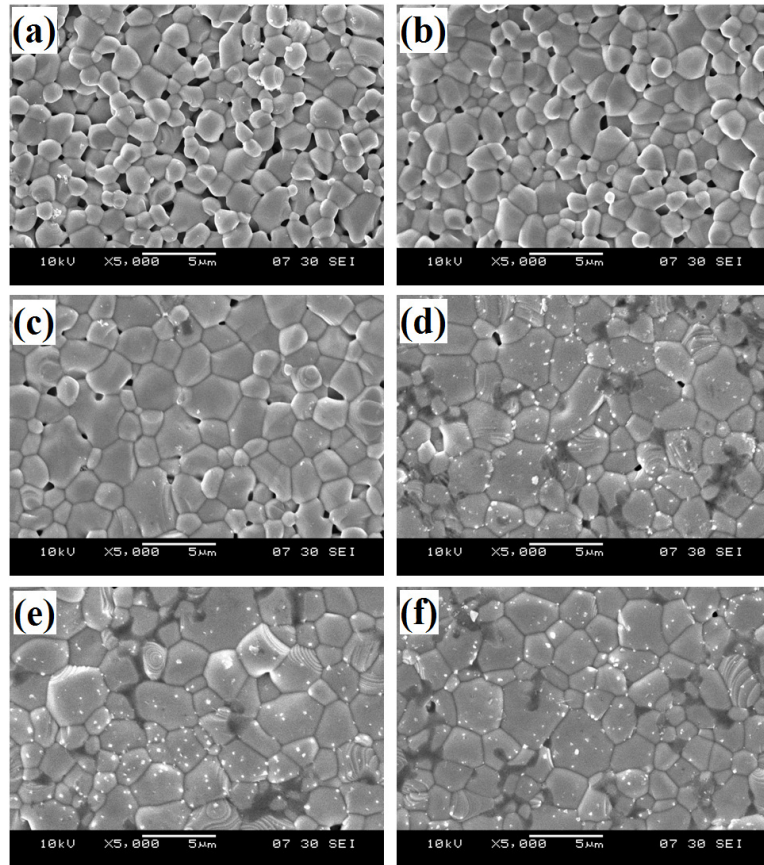


Figure 1: Typical SEM images of (a) as-grown ZnO discs, and annealed at (b) 450°C, (c) 550°C, (d) 650°C, (e) 750°C and (f) 850°C temperatures.

Interestingly, tiny, distinct white spots of ZnO nanoparticles (approximately 80 nm to 100 nm) were found on the specimens, particularly for the 850°C sample shown in Figure 1(f). At a very high annealing temperature, the atoms have enough diffusion activation energy to occupy the correct site in the crystal lattice and the free zinc in the samples have a high energy to interact with oxygen during the annealing process which in turn leads to the appearance of the large white spots during annealing in this temperature. The larger white spots may be the agglomerates of ZnO nanoparticles. Excess zinc naturally produced from sintered ZnO may have provided this free zinc that was oxidised into ZnO during the oxygen-rich annealing treatment. The EDX spectra [inset of Figure 2(f)] for the white spots in samples annealed at 850°C show that presence of only Zn and O, suggesting pure ZnO nanoparticle composition of this white spots.

Figure 1 also shows the layer-by-layer growth of several grains. The growth of the secondary layer occurred during the oxygen-rich annealing, particularly at temperatures above 650°C. This polycrystalline layer is approximately 80 nm to 120 nm thick. The growth of the secondary layer may have been due to a high concentration of free zinc in the localised grains exhibiting multilayer growths.

Significant grain growth occurred in the ZnO discs even at a low annealing temperature (450°C), in addition to a secondary growth involving ZnO nanoparticles and multilayer grains. This interesting phenomenon may be attributed to the strong surface reaction during annealing due to the very large surface area of the 20 nm nanoparticles used in creating the ZnO discs. Increasing the annealing temperature resulted in the compression of the ZnO grains towards the centre of the disc and the growth of grain size. The increased annealing temperature was led to the oxygen concentration in the disc and caused a distortion in the form of the grains; this result indicates the presence of tensile stress in ZnO discs.

The EDX scan data (Figure 2) for the all area show that the oxygen content in the ZnO discs increased with increasing annealing temperature because of the increase in the oxygen diffusion energy. The observed high oxygen content in the annealed sample may be attributed to the interaction of ZnO with atmospheric oxygen during the annealing process under ambient conditions. The EDX results also reveal the presence of trace amounts of other elements such as Si (impurities) in the ZnO discs, which were introduced during the preparation and annealing processes.

The XRD spectra (Figure 3) of the ZnO disc specimens are characterised by major peaks at (101), (100), (002) and (110), which confirm the polycrystalline nature of the discs. The increase in the annealing temperature resulted in higher and narrower diffraction peaks with smaller full-widths at half-maximum (FWHM), indicating better crystallinity, as observed in the sample annealed at 850°C [Figure 3(f)]. This result is in contrast to the lower intensity peaks of the sample annealed at 450°C [Figure 3(b)].

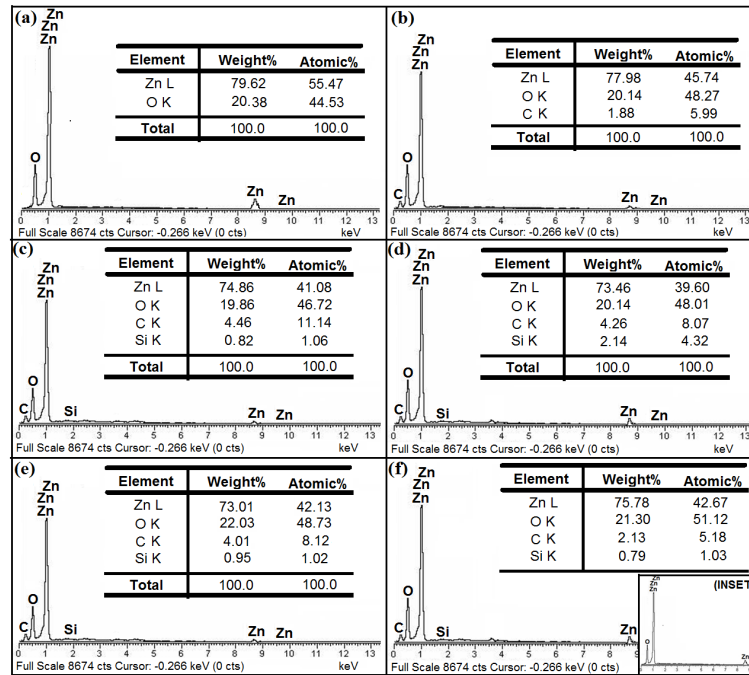


Figure 2: EDX spectra of (a) as-grown ZnO discs, and annealed at (b) 450°C, (c) 550°C, (d) 650°C, (e) 750°C and (f) 850°C temperatures.

The intense (101) peak of the as-grown ZnO disc increased from $2\theta = 36.10^\circ$ to $2\theta = 36.14^\circ$ after annealing at 450°C, indicating the occurrence of residual stress in the ZnO disc. The (101) peak (Figure 4) became narrower, less asymmetric and gradually shifted to higher 2θ values as the annealing temperatures increased, which resulted in the decrease in the lattice constant (Table 1). Moreover, the FWHM of the (101) diffraction peak decreased with the increasing temperature (Table 1), suggesting that the thermal annealing temperature improved the crystallisation of the ZnO nanoparticles.

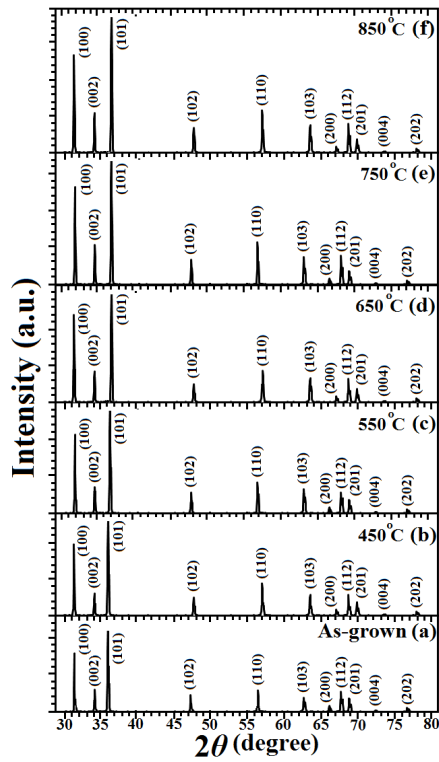


Figure 3: XRD patterns of (a) as-grown ZnO discs, and annealed at (b) 450°C, (c) 550°C, (d) 650°C, (e) 750°C and (f) 850°C temperatures.

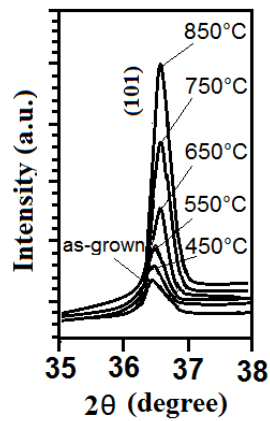


Figure 4: An enlarged view of the (101) X-ray diffraction peak of ZnO discs showing a shifting of this peak at different annealing temperatures.

Table 1: Summarised data from SEM images, XRD patterns and PL spectra.

Annealing temperature	SEM		XRD				PL peak			
	Grain size (μm)	2θ ($^\circ\text{C}$)	a (\AA)	c (\AA)	FWHM ($^\circ\text{C}$)	Stress (σ) (G.Pa)	Wave-length (nm)	Energy band-gap (eV)	Wave length (nm)	Band peak energy (eV)
As-grown	1.3	36.10	3.253	5.217	0.295	-0.941	365.53	3.392	527.97	2.349
450 $^\circ\text{C}$	1.4	36.14	3.251	5.215	0.258	-0.767	365.14	3.396	526.17	2.356
550 $^\circ\text{C}$	1.6	36.15	3.250	5.211	0.199	-0.418	365.03	3.397	526.04	2.357
650 $^\circ\text{C}$	1.9	36.19	3.249	5.205	0.198	0.105	368.67	3.363	540.91	2.292
750 $^\circ\text{C}$	2.4	36.21	3.245	5.203	0.198	0.279	369.22	3.358	545.21	2.274
850 $^\circ\text{C}$	2.7	36.27	3.242	5.195	0.197	0.976	369.85	3.353	550.33	2.253

The stress in the ZnO discs may have been introduced via two mechanisms. One is that the intrinsic stress is due to the crystallite deficiency during growth, as well as the impurities and defects in the discs. Another is that the growth parameters, such as pressure, gas mixture, power and deposition temperature, may have caused the intrinsic stress. Previous studies^{9,15} have revealed that the intrinsic stress of the as-grown ZnO is compressive. By contrast, extrinsic stress can be generated during pressing, sintering, and annealing processes. The thermal stress in the discs results from the difference in the coefficient of thermal expansion α due to the variations in the annealing temperature.

The magnitude of the compressive stress component during the growth process was increased until it was converted to the thermal (tensile) stress component at a very high annealing temperature; therefore, an overall compressive residual stress was observed in the as-grown ZnO. The increase in the tensile stress with increasing temperature may be attributed to the increasing diffusion rate of oxygen on the surface of the disc, as well as the increase in the rate of reaction between the free Zn in the sample and oxygen at high annealing temperatures, which lead to an increase in the oxygen concentration in the ZnO disc. On the other hand, increasing the annealing temperature increased the energy for the diffusion of oxygen in the ZnO disc, which leads to tension in the lattice constant during the growth process.

The lattice constant (c) of the ZnO samples was obtained from the peak positions of the ZnO (002) planes. The results are summarised in Table 1. These values are comparable to the lattice constants of bulk ZnO (c_0) at 5.208 \AA .¹⁶ Using these data, the stress (σ) in the ZnO disc was calculated using the strain model for hexagonal crystals, as shown in Equation 1:^{17,18}

$$\sigma = \left(\frac{2C_{13}^2 - C_{33}(C_{11} - C_{12})}{C_{13}} \right) \left(\frac{C_0 - c}{C_0} \right) \quad (1)$$

where $C_{11} = 209.7$ GPa, $C_{12} = 121.1$ GPa, $C_{13} = 105.1$ GPa, $C_{33} = 210.9$ GPa, c_0 and c refer to the mean stress in the ZnO sample, the elastic stiffness constants of bulk ZnO, the lattice constant of strain-free bulk ZnO and the lattice constant of the ZnO disc, respectively. The numerical value of the elastic stiffness constants of bulk ZnO is approximately -453.6 GPa. The estimated values for σ in the ZnO disc for the (002) plane grown at different annealing temperatures are listed in Table 1. The increasing order of the stress values is as follows: $\sigma(a) < \sigma(b) < \sigma(c) < \sigma(d) < \sigma(e) < \sigma(f)$. The negative value of the compressive stress indicates that the lattice constant is elongated compared with that of the stress-free sample.¹⁶ The positive values of samples d, e, and f indicate a tensile stress that results from the stretching crystal size, indicating that the lattice constant decreased compared with that of the stress-free sample.

The photoluminescence (PL) spectra in [Figure 5(a)] show two emission bands for the ZnO discs, particularly in the UV and blue-green-red regions. The UV emissions with band peaks at 365 nm to 369 nm have lower intensities compared with the broad, visible band peaks at 527 nm to 550 nm. The characteristic UV band edge PL peak of the as-grown ZnO disappeared as the annealing temperature increased because of the high intensity of the blue-green-red emission.^{19,20} The broad visible emission may be attributed to the electronic transitions from the near-conduction band edge to deep level acceptors, as well as to the transitions from the deep donor levels to the valence band.²¹ The visible emission was produced from the recombination of shallowly trapped electrons with deeply trapped holes in the V_o^{++} centres.²² Previous studies^{23,24} have attributed the increase in the green emission to Zn/O interstitial centres.

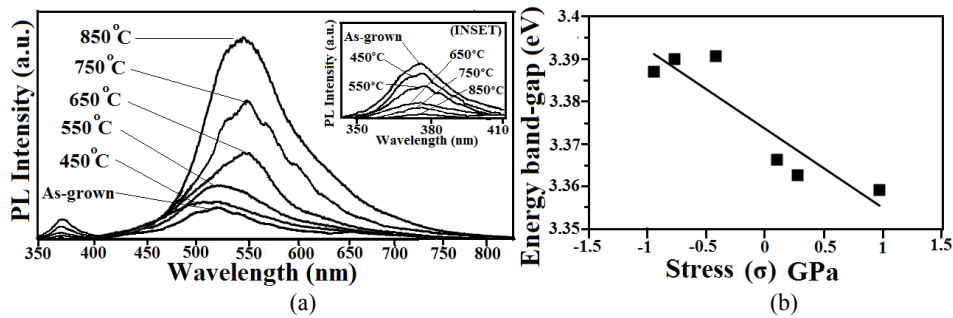


Figure 5: Illustration of (a) PL spectra of ZnO discs at different annealing temperatures in the visible region and in the UV region (INSET), and (b) variation of the band-gap energy as a function of the different stress on the ZnO discs.

In the current study, the increase in the blue-green-red visible PL emission may be attributed to an extremely high concentration of structural defects in the starting raw material (20 nm ZnO nanoparticles). The structural defects were intrinsic (oxygen vacancies and zinc interstitials) and acted as deep-level acceptors for electronic transitions with the near-conduction band edge.

The broad PL visible emission of the samples increased as the high-oxygen annealing temperature increased, whereas the UV emission decreased [Figure 5(a)]. Oxygen absorption on the ZnO disc surface may have increased as the annealing temperature increased from 450°C to 850°C and may have driven the photogenerated electron-hole pairs in the depletion region to move to opposite directions.²⁵ The enhanced oxygen absorption at high annealing temperatures (450°C and 550°C) also caused a blueshift in the PL emission peaks of ZnO, which may be attributed to compressive stress. The blueshift turned into a redshift when the annealing temperature was increased to 650°C, 750°C and 850°C, resulting in an increase in stress. As a result, the bandgaps of the ZnO nanoparticles decreased with increasing annealing temperature, and the tensile stress became more dominant as the grain size increased. The shift in the band-gap energy is related to the structural property. The inherent tensile strain in the ZnO disc can be relaxed by providing sufficient thermal energy, which lowers the band-gap energy. The band-gap was found to vary within the 450°C to 850°C annealing temperature range, which agrees with the reported value.²⁶ The variation in the energy band-gap as a function of stress was measured (Table 1) and plotted in Figure 5(b) to determine the effect of stress on the energy band-gap. The band-gap energy can be determined using the following equation:

$$E_g = \frac{hc}{\lambda} \quad (2)$$

where E_g = band-gap energy, h is Planck's constant and c is light speed.

The variation in the energy band-gap and stress with different annealing temperatures is shown in Figure 6. The observed shift in the energy band-gap from a higher to a lower value may be attributed to the conversion of the compressive stress to a tensile stress with increasing annealing temperature. A decrease in the UV emission peak was observed at higher annealing temperatures as the compressive stress increased because of the increase in the grain size. Hence, the variation in the band-gap with temperature significantly correlated with the stress in the disc, indicating that the increase in the annealing temperature induced an increase in the grain size, and caused a reduction in the quantum size effect (or in the energy band-gap) in the ZnO nanoparticles.^{14,27,28} At the same time, the increased temperature promoted the diffusion of oxygen on

the discs and led to a decrease in the ZnO lattice constant, consequently increasing the tensile stress in the sample.^{16,27,29}

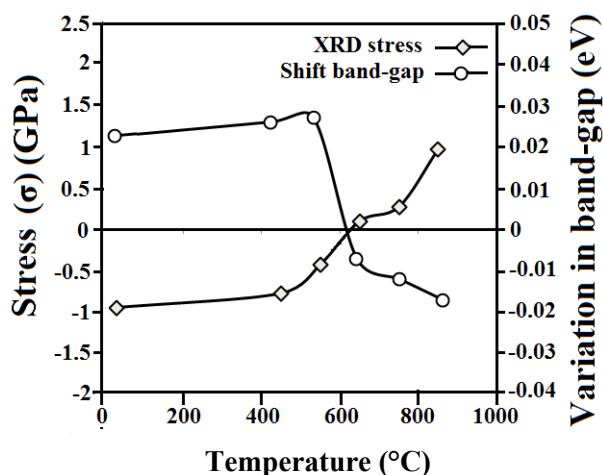


Figure 6: Variation in band-gap ($E_{g_{\text{bulk}}} - E_g$) and stress in the ZnO discs with different annealing temperature.

This study shows that a decrease in the PL emission peaks and energy bandgap with increasing annealing temperature plays an important role in increasing the stress. Similar results were also obtained using Raman spectroscopy and SEM, indicating that the stress significantly affects the structural and optical properties of ZnO nanoparticles.

Figure 7 shows the Raman spectra for the ZnO discs at different thermal annealing temperatures. Raman scattering is very sensitive to the microstructure and can be used to obtain additional information on the structure of the ZnO nanoparticles. Single-crystalline ZnO has eight sets of optical phonon modes at the Γ point of the Brillouin zone, wherein the Raman active modes are $E_2^{(\text{low})}$, $E_2^{(\text{high})}$, $A_1(\text{TO})$, $E_1(\text{TO})$, $A_1(\text{LO})$ and $E_1(\text{LO})$. Generally, the $E_2^{(\text{high})}$ optical phonon mode of the ZnO nanoparticle represents a wurtzite structure. Compared with the stress-free bulk ZnO (437 cm^{-1}),³⁰ the different positions and intensity of the $E_2^{(\text{high})}$ mode (shifting up or down) indicate a change in the band structure of the ZnO nanoparticles and provide information on the stress. In a similar manner, an increase in the $E_2^{(\text{high})}$ phonon frequency indicates the occurrence of compressive stress in the crystal, whereas a decrease in this mode is attributed to tensile stress.³¹ The $E_2^{(\text{high})}$ positions for the discs annealed at 450°C and 550°C were observed at 439.4 cm^{-1} and 438.6 cm^{-1} , respectively, indicating an upward shift of approximately 2.4 cm^{-1} and 1.6 cm^{-1} . The upward shift in the position of the $E_2^{(\text{high})}$ phonon mode is attributed to the compressive stress in the ZnO discs. On the other hand, the position of the $E_2^{(\text{high})}$ phonon mode for the discs annealed

at 650°C, 750°C and 850°C shifted downward to 436.8 cm⁻¹, 436.2 cm⁻¹ and 435.1 cm⁻¹ (corresponding to shifts of 0.2 cm⁻¹, 0.8 cm⁻¹ and 1.9 cm⁻¹), respectively, indicating the occurrence of tensile stress in the ZnO discs, which increased with temperature. Two Raman-active optical phonons were assigned in all the annealed samples. The peaks appearing at 110 cm⁻¹ and 595 cm⁻¹ correspond to the E₂^(low) and E₁(LO) phonon modes of ZnO, respectively. The E₁(LO) peak centred at 595 cm⁻¹ is attributed to the formation of defects such as oxygen vacancies and Zn interstices.³¹

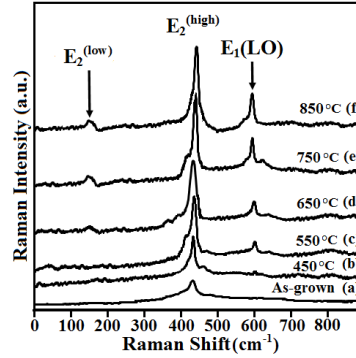


Figure 7: Raman spectra of (a) as-grown ZnO discs, and annealed at (b) 450°C, (c) 550°C, (d) 650°C, (e) 750°C and (f) 850°C temperatures.

4. CONCLUSION

ZnO discs were prepared via the conventional ceramic processing method and then annealed at different temperatures. SEM, EDX and XRD were used to characterise the disc morphologies and crystal structures of the samples. The crystal quality of the ZnO discs was highly dependent on the annealing temperature. Increasing the annealing temperature from 450°C to 850°C resulted in a larger grain size and improved grain crystallinity, as indicated by the decreased intrinsic compressive stress deduced from the XRD lattice constant and FWHM data. The XRD analysis at 2θ shows that the ZnO disc suffers from a slight compressive stress at low annealing temperatures; this stress is then converted to tensile stress and gradually increases with increasing temperature. The PL spectra of the ZnO nanoparticle show the effect of stress on the energy bandgap. The change trend of the energy bandgap relative to the as-grown ZnO indicates a change in the band structure of the ZnO nanoparticles and provides information on the stress. The upward shift in the energy bandgap corresponds to the occurrence of compressive stress in the crystal, whereas the decreased value of this bandgap is due to tensile stress. The shift in the E₂^(high) optical phonon mode of the ZnO nanoparticles indicates the effect of stress on the wurtzite

structure. All these results indicate that high-oxygen thermal annealing can be used as a new technique in controlling the different properties of nanoparticle-based ZnO discs and obtain high-quality discs with improved structural properties and minimal stress.

5. ACKNOWLEDGEMENT

This work was supported by an APEX grant (1002/PFIZIK/910305) from Universiti Sains Malaysia (USM). We express gratitude to the Cultural Mission of the Royal Embassy of Saudi Arabia. We further acknowledge the priceless assistance from the Nano-Optoelectronics Research and technology Laboratory (NOR Lab) of USM.

6. REFERENCES

1. Miao, L., Tanemura, S., Yang, H. Y. & Lau, S. P. (2009). Synthesis and random laser application of ZnO nano-walls: A review. *J. Nanotech.*, 6, 723–734.
2. Xu, C. X. & Sun, X. W. (2003). Field emission from zinc oxide nanopins. *Appl. Lett.*, 83, 3806–3808.
3. Xu, C. X., Sun, X. W. & Chen, B. J. (2004). Field emission from gallium-doped zinc oxide nano fiber array. *Appl. Phys. Lett.*, 84, 1540–1542.
4. Zhao, M. H., Wang, Z. L. & Mao, S. X. (2004). Piezoelectric characterization individual zinc oxide belt probed by piezoresponse force microscope. *Nano Lett.*, 4, 587–590.
5. Arnold, M. S., Avouris, P., Pan, Z. W. & Wang, Z. L. (2003). Field-effect transistors based single semiconducting oxide nanobelts. *J. Phys. Chem.*, 107(3), 659–663.
6. Huang, M. H. et al. (2001). Catalytic growth of zinc oxide nanowires by vapor transport. *Adv. Mater.*, 13, 113–116.
7. Mahmud, S. (2011). One-dimensional growth of Zinc oxide nanostructures from large micro- particles in a highly rapid synthesis. *J. Alloy. Compd.*, 509, 4035–4040.
8. Fang, Z. B. et al. (2005). Influence of post- annealing treatment on the structure properties of ZnO films. *Appl. Surf. Sci.*, 241, 303–308.
9. Wang, M. et al. (2006). Effect of preheating and annealing temperatures on quality characteristics of ZnO thin film prepared by sol-gel method. *Mater. Chem. Phys.*, 97, 219–225.

10. Hong, R. J. et al. (2005). Influence of different post treatments on the structure and optical properties of zinc oxide thin films. *Appl. Surf. Sci.*, 242, 346–352.
11. Cui, M. L., Wu, X. M., Zhuge, L. J. & Meng, Y. D. (2007). Effects of annealing temperature on the structural and photoluminescence properties of ZnO films. *Vacuum*, 81(7), 899–903.
12. Liu, Y. C. et al. (2006). Influence of annealing on optical properties and surface structure of ZnO thin films. *J. Crystal Growth*, 287(1), 105–111.
13. Wang, C. et al. (2007). Effects of oxygen pressure on the structure and photoluminescence of ZnO thin films. *J. Mater. Sci.*, 42, 9795–9800.
14. Mahmood, A. et al. (2010). Effect of thermal annealing on the structural and optical properties of ZnO thin films deposited by the reactive e-beam evaporation technique. *Phys. Scr.*, 82(6), 065801, doi:10.1088/0031-8949/82/06/065801.
15. Maniv, S., Westwood, W. D. & Colombini, E. (1982). Pressure and angle of incidence effects in reactive planar magnetron sputtered ZnO layers. *J. Vac. Sci. Technol.*, 20(2), 162–170.
16. Reeber, R. R. (1970). Lattice parameters of ZnO from 4.2° to 296° K. *J. Appl. Phys.*, 41, 5063–5066.
17. Zhang, Z., Chen, X., Zhang, X. & Shi, C. (2006). Synthesis and magnetic properties of nickel and cobalt nanoparticles obtained in DMF solution. *Solid State Commun.*, 139, 403–405.
18. Zhang, W. C. et al. (2008). Excitation wavelength dependence of the visible photoluminescence from amorphous ZnO granular films. *J. Appl. Phys.*, 103(9), 3718–3723.
19. Hung, C. H. & Whang, W. T. (2005). Effect of surface stabilization of nanoparticles on luminescent characteristics in ZnO/poly (hydroxyethylmethacrylate) nanohybrid films. *J. Mater. Chem.*, 15, 267–274.
20. Zeng, H. et al. (2006). Violet photoluminescence from shell layer of Zn/ZnO core-shell nanoparticles induced by laser ablation. *Appl. Phys. Lett.*, 88(17), 910–912.
21. Sui, X. M., Shao, C. L. & Liu, Y. C. (2005). White light emission of polyvinyl alcohol/ZnO hybrid nanofibers prepared by electrospinning. *Appl. Phys. Lett.*, 87(11), 3115–3117.
22. Van Dijken, A., Meulenkamp, E. A., Vanmaekelbergh, D. & Meijerink, A. (2000). The kinetics of the radiative and nonradiative processes in nanocrystalline ZnO particles upon photoexcitation. *J. Phys. Chem. B*, 104, 1715–1723.
23. Mishra, K. C. et al. (1990). Bands versus bonds in electronic-structure theory of metal oxides: Application to luminescence of copper in zinc oxide. *Phys. Rev. B*, 42, 1423–1430.

24. Reynolds, D. C., Look, D. C., Jogai, B. & Morkoc, H. (1997). Similarities in the bandedge and deep-center photoluminescence mechanisms of ZnO and GaN. *Solid State Commun.*, 101(9), 643–646.
25. Moulder, J. F. et al. (1992). *Handbook of X-ray photoelectron spectroscopy*. Minnesota: Perkin-Elmer.
26. Kumar, R., Khare, N., Kumar, V. & Bhalla, G. L. (2008). Effect of intrinsic stress on the optical properties of nanostructured ZnO thin films grown by rf magnetron sputtering. *Appl. Surf. Sci.*, 254, 6509–6513.
27. Kim, K. K. et al. (2004). Fabrication of ZnO quantum dots embedded in an amorphous oxide layer. *Appl. Phys. Lett.*, 84, 3810–3812.
28. Ghosh, R., Bask, D. & Fujihara, S. (2004). Ultraviolet photodetection properties of a Pt contact on a Mg_{0.1}Zn_{0.9}O/ZnO composite film. *J. Appl. Phys.*, 96, 2689–2692.
29. Scepanovic, M. et al. (2010). Raman study of structural disorder in ZnO nanopowders. *J. Raman Spectr.*, 41, 914–921.
30. Segura, A. et al. (2003). Optical properties and electronic structure of rock-salt ZnO under pressure. *Appl. Phys. Lett.*, 83(2), 278–280.
31. Jeong, S. H., Kim, J. K. & Lee, B. T. (2003). Effects of growth conditions on the emission properties of ZnO films prepared on Si(100) by rf magnetron sputtering. *J. Phys. D*, 36(16), 2017–2020.
32. Lin, Y. et al. (2005). Green luminescent zinc oxide films prepared by polymer-assisted deposition with rapid thermal process. *Thin Solid Films*, 492, 101–104.